

THE MAGNET LATTICE OF THE POHANG LIGHT SOURCE STORAGE RING

M. Yoon, J. Choi, T. Lee, and G. Kim
 Pohang Accelerator Laboratory,
 Pohang Institute of Science and Technology,
 Pohang, Korea 790-600

Abstract

The storage ring lattice of the Pohang Light Source (PLS) employs a 12 superperiod, mirror symmetric Triple Bend Achromat (TBA) structure. There are total six quadrupoles per each half cell, three in the non-dispersive section and three in the dispersive section. A study for linear and nonlinear beam optics has been performed. This includes the study of effects due to the closed orbit distortion, multipole error, and insertion devices. Results of these investigations are summarized here.

Introduction

Third generation synchrotron light sources are characterized by small emittance and long straight sections for wigglers and undulators. For the storage ring of PLS, a 12-superperiod TBA lattice is chosen. One characteristic feature of the PLS lattice is that the bending magnet does not employ a gradient. This leads to larger natural emittance than that of other third generation light sources. The circumference of the storage ring is 280.56 m. Per each superperiod, there are three bending magnets. With bending field of 1.058 T the critical photon energy from the bending magnet is 2.8 keV. In table I are listed the major storage ring parameters for the PLS. Fig.1 shows betatron and dispersion functions for one superperiod of the PLS lattice.

Nonlinear effects

For the nominal operation of the PLS storage ring, the natural chromaticity, $(\xi_x, \xi_y) = (-23.36, -18.19)$ is corrected to zero by a pair of sextupoles, $(SD, SF) = (-6.47662 \text{ m}^{-2}, 4.49238 \text{ m}^{-2})$. These sextupole strengths are considerably smaller than those for other third-generation light sources.

Table I Major storage ring parameters

Nominal Energy (GeV)	2
Superperiods	12
Circumference (m)	280.56
Harmonic Number	468
RF Frequency (MHz)	500.087
Natural Emittance at 2.0 GeV (nm-rad)	12.1
Natural Chromaticity (h/v)	-23.36/ -18.19
Number of Sextupole Families	2
Length of the Insertion Straight (m)	6.8
Betatron Tunes (h/v)	14.28/8.18
Energy Spread, $\sigma_E (= \delta E/E)$	0.00068(0.00085)
Natural Energy Spread	0.00068
Momentum Compaction	0.00181
Synchrotron Tune	0.0109688
Natural Bunch Length (mm)	5.03953
Damping Times (ms)	
Horizontal	16.62
Vertical	16.62
Longitudinal	8.34
Effective Length of the Dipole Magnet (m)	1.1
Dipole Field at 2.0 GeV (T)	1.058

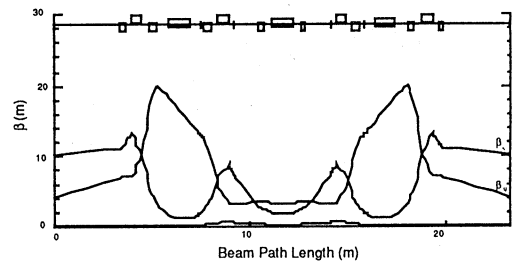


Fig. 1 Twiss parameters for one cell of the PLS lattice

The chromaticity correction sextupoles induce amplitude-dependent tune shifts, thus making the motion of particles with large oscillation amplitudes unstable. The region of the stable amplitude, the dynamic aperture, can be obtained utilizing a particle tracking code. Fig. 2 shows the dynamic aperture for zero momentum deviation obtained from the tracking code MAP¹ for 1,000 turns.

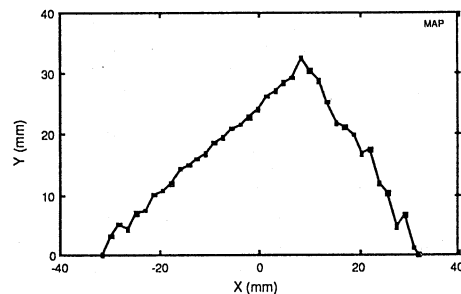


Fig. 2 Dynamic aperture with chromaticity correction sextupoles

The chromaticity correction sextupoles also induce the nonlinear momentum-dependent tune shifts. Our study indicated that the deviation of tunes from the nominal values are relatively small up to $\pm 4\%$ momentum deviation².

The magnet multipole components are denoted as

$$B(x, y) = B_y + iB_x = B\rho \sum_{n=1} (b_n + a_n)(x + iy)^{n-1},$$

where b_n and a_n denote normal and skew components respectively. For the values for multipole coefficients, a_n and b_n , we referred to ALS values³ and slightly modified them considering the difference in the magnet design. These multipole components reduce the dynamic aperture via amplitude-dependent tune shifts. To evaluate the reduction, particle tracking was performed up to 300 turns with the program RACETRACK. For random components, Gaussian distribution was assumed and the truncation was made at ± 2 sigma. The results of the particle tracking are displayed in Fig. 3. This figure shows the dynamic aperture averaged over 10 different machines when all the systematic and random errors are applied as input for the tracking simulations.

It is seen from the figure that there is some reduction in the dynamic aperture, though the reduction is not great.

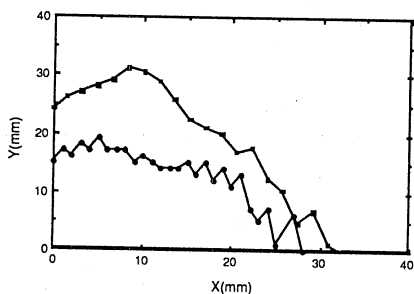


Fig. 3 Dynamic apertures with and without random and systematic multipole errors

Closed orbit distortions and corrections

To get a realistic estimation of the closed orbit distortion, we have simulated by MAD6 and RACETRACK with 20 different storage ring models, each with a different set of random errors with Gaussian distribution truncated at $\pm 2\sigma$. The tolerance values are taken to be $\Delta B/B$ (bending magnet field error) = 0.1 %, $\Delta x = \Delta y$ (quadrupole misalignment) = 0.15 mm, $\Delta\phi$ (bending magnet rotation error) = 0.5 mrad. The orbit distortions are monitored through 108 beam position monitors (9 per cell) and corrected by 7 horizontal and 7 vertical correctors per cell. Among them 6 correctors are horizontal and vertical combined function magnets. The other horizontal and vertical correctors are trim windings on the sextupoles. In the PLS, all sextupole magnets have corrector trim windings. In the simulation, however, only one horizontal and one vertical trim winding are assumed to be used, because these trim windings on sextupoles generate spurious random sextupole and decapole components.

Since there is no space for correctors in the injection straight section, the total number of correctors used in the simulation is 82 each. There are horizontal corrector trim windings on bending magnets and these will be activated in the injection and RF regions. The trim windings on bending magnets have not been taken into account in our simulation. The position of correctors and monitors in a normal cell is shown in Fig. 4. Fig. 5 shows the rms orbit distortions produced by 20 sets of random errors before and after correction and also with and without monitor reading errors of 0.15 mm rms. The MICADO algorithm included in MAD6 was used.

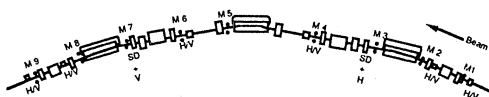


Fig. 4 The position of correctors and monitors in a normal cell

Due to the rather large sextupole strengths for chromaticity correction, and the uncorrected closed orbit distortion for the PLS lattice, one expects a large change in tune, a typical feature of third-generation synchrotron radiation source storage rings. Therefore, a reduction in dynamic aperture is expected. The dynamic apertures before correction have been calculated for 10 different ring models, the averaged result of which is shown in Fig. 6. The program RACETRACK was utilized and tracking

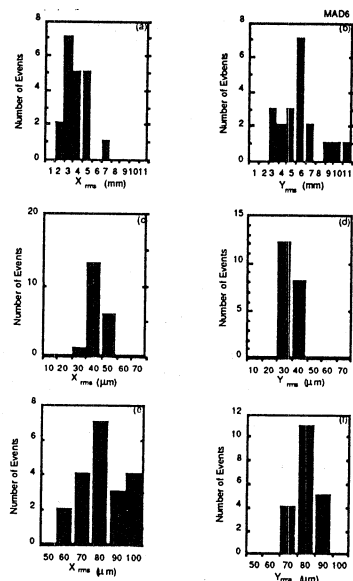


Fig. 5 The rms orbit distortions by 20 sets of random errors. (a),(b): before correction (c),(d): after correction without monitor error (e),(f): after correction with monitor error (MICADO method)

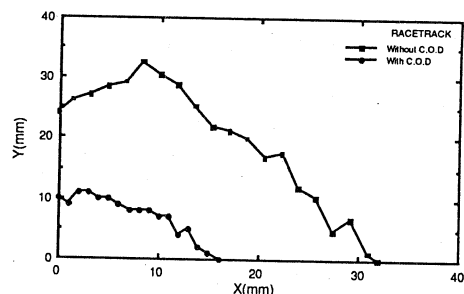


Fig. 6 Dynamic aperture with closed orbit distortions

Around the storage ring, there are many vibration sources which affect the beam motion. The most stringent requirement for orbit control comes from the photon beam from an undulator where the spectral brightness B is important. The spectral brightness is directly related to the emittance of the electron beam. To prevent a qualitative deterioration of the photon beam, we have a provision to measure the position and angle of the photon beam downstream, and can correct the electron beam locally. In order to correct both the angle and the position of the beam, two corrector magnets are required upstream. Two corrector magnets placed downstream then restore the orbit to the normal closed orbit. We set the frequency of this feedback to be 25 Hz. The vibrational sources which have frequencies higher than 25 Hz should be corrected at the sources themselves or at least minimized by special means.

Another consideration for the closed orbit correction in the PLS is fast global orbit correction. Recently, the successful operation of a real time global orbit correction has been performed at the NSLS storage ring⁴. The method is based on harmonic orbit correction. Since the orbit distortion is most sensitive to the machine tune, one can activate the correctors in such a way that the dominant harmonics are cancelled. Among many monitors and correctors, particular correctors and monitors can be selected to be used for the fast global correction. The frequency for this correction can be around 10 Hz.

Effects of wigglers and undulators

Insertion devices not only break the linear optics of the lattice, but also introduce higher order field components that may excite non-systematic resonances. Passing through the vertical field variation of insertion devices, closed paths are wiggled in the horizontal direction, which implies non-linear magnetic interaction as well as additional linear vertical focusing. Hence insertion devices induce changes in tune and the betatron function, and break the condition, $\alpha = 0$, that is necessary for periodic closed orbit formation. As a result, the dynamic aperture can be significantly reduced.

The linear optics distortion can be recovered to some extent by controlling the three pairs of quadrupoles surrounding the injection straight region. Two pairs of quadrupoles are used to recover the condition $\alpha = 0$ (α matching) and the other pair is used to minimize $\sqrt{\Delta\nu_x^2 + \Delta\nu_y^2}$ (tune matching), where $\Delta\nu$ is the tune change by insertion devices. Even though the non-linear interactions still exist and reduce the dynamic aperture greatly, these matchings improve the situation. Table II shows the insertion device parameters used for our calculation and Table III shows the corresponding linear optics distortions. To obtain the dynamic aperture, the program RACETRACK was utilized.

Table II List of insertion device parameters

	Undulator	Wiggler
Field Parameter (K)	2.5	28
Period (λ) (cm)	5	14
Number of Periods (N)	80	14
Peak Field (B_0) (T)	0.5	2.0
Length (L) (m)	4	1.96

Fig. 7 shows the dynamic apertures with α matching and both α and tune matching when one wiggler of Table II is used.

Table III Tune changes with ID

ID	α matching	α and tune matching
Wiggler	$\nu_x=14.2770, \nu_y=8.2551$	$\nu_x=14.2480, \nu_y=8.1901$
Undulator	$\nu_x=14.2793, \nu_y=8.1754$	$\nu_x=14.2764, \nu_y=8.1805$

Injection

The length of the injection straight is 6.8 m. Along this injection straight, four bump magnets and one Lambertson septum magnet are placed. The incoming electron beam from the beam transfer line is horizontally parallel with the storage ring bumped orbit and it is injected 8 degrees vertically. The Lambertson magnet then bends the beam -8 degrees vertically to

place it on the same level as the bumped orbit. We take the bumped orbit to be 21 mm. By taking 0.74 m for the effective length of the bump magnet and 1.26 m for the distance between the centers of the first two bump magnets, the required magnetic field for a bump magnet to produce 21 mm bumped orbit

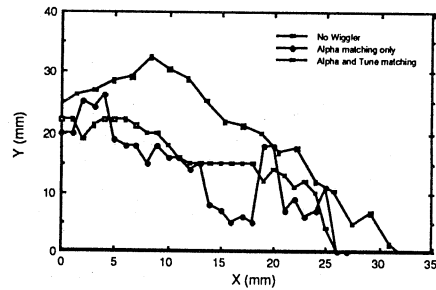


Fig. 7 Dynamic apertures with one wiggler

is found to be 1.5 kG at 2 GeV. The kick angle of the bump magnet is then 16.64 mrad. Considering that the bump magnet may have a difficulty in producing 21 mm bumped orbit, we have a provision for activating the horizontal trim windings on the upstream and downstream bending magnets.

The bump magnet is operated with 10 Hz repetition rate. It has a 4 μ sec half-sine wave so that the rise and fall time are both 2 μ sec. Thus the injected beam will restore the original stored orbit in less than three orbital turns (the revolution time of the storage ring beam is 0.94 μ sec). The Lambertson magnet is 1.17-m long and the maximum field was chosen to be 8 kG. The bending angle is, therefore, 8 degrees.

In the drift space between the Lambertson magnet and the downstream bump magnet (bump 3), the injected beam profile will be measured using a destructive profile monitor. The enclosure for the placement of this monitor will be kept at low vacuum (about 10^{-3} torr).

References

- 1 Unpublished computer program by M. Yoon
- 2 PLS Design Report, to be published
- 3 ALS Conceptual Design Report PUB-5172 1986
- 4 L.H. Yu et al. Nuclear Instruments and Methods in Physics Research A284 (1989) 268-285